Case Studies in Construction Materials 21 (2024) e03691

Contents lists available at ScienceDirect

Case Studies in Construction Materials

journal homepage: www.elsevier.com/locate/cscm

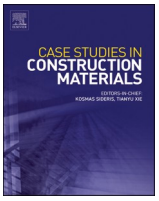

Thermal, electrical, and mechanical performances of ultrahigh-performance cementitious composites with multiwalled carbon nanotubes

Sunho Kang [a], Sukhoon Pyo [b], Heeyoung Lee [c,*]

[a] Chosun University, Republic of Korea
[b] Department of Civil, Urban, Earth, and Environmental Engineering, Ulsan National Institute of Science and Technology (UNIST), Republic of Korea
[c] Department of Civil Engineering, Chosun University, Republic of Korea

ARTICLE INFO

Keywords:
Multifunctional performance
Multiwalled carbon nanotube
Ultrahigh-performance cement
Thermal performance
Electrical resistance

ABSTRACT

This study examines the influence of multiwalled carbon nanotubes (MWCNTs) on cementitious composites, specifically focusing on the fabrication of multifunctional cementitious composites known as ultrahigh-performance cementitious (UHPC) composites. Key properties such as compressive strength, thermal performance, and electrical resistance were examined with varying MWCNT contents, curing methods, curing duration, and supply voltage. The effects of the incorporation of MWCNTs on the hydration reactions of the cementitious composites were analyzed using field-emission scanning electron microscopy, thermogravimetric analysis, and X-ray diffraction. The study revealed that MWCNT UHPC composites can achieve a maximum ultrahigh strength of 120.8 MPa. Additionally, the incorporation of MWCNTs enabled the composites to reach a maximum surface temperature of 90.6 °C during heating. Furthermore, the power consumption of MWCNT UHPC composites was found to be predictable based on the curing type and the duration of curing. Notably, the hydration reactions in MWCNT UHPC composites remained unaffected by the MWCNT content. The findings emphasize the potential of multifunctional MWCNT UHPC composites by offering exceptional strength, heating capabilities, and electrical performance in construction materials.

1. Introduction

Several studies have been conducted to assess the effects of carbon nanotubes (CNTs) on the physical and chemical properties of cementitious composites, materials, and concrete [1–7]. Nanomaterials have attracted significant attention owing to their exceptional electrical and thermal properties [8–12]. CNTs are classified into two main categories, namely single-walled CNTs (SWCNTs) and multi-walled CNTs (MWCNTs). Mahanthesh et al. [13] investigated MWCNT and SWCNT solutions based on magnetohydrodynamic flow measurements. The researchers analyzed the impact of these solutions on the thermal performance of composites based on flow velocity and distribution. The findings revealed that the MWCNT solution had superior heat transfer performance solution compared with that of the SWCNT solution. Lee et al. [14] fabricated cement composites by formulating solutions containing MWCNTs and

* Correspondence to: Department of Civil Engineering, College of Engineering, Chosun University, 309 Pilmun-Daero, Dong-Gu, Gwangju, Republic of Korea.
E-mail addresses: lineho@chosun.ac.kr (S. Kang), shpyo@unist.ac.kr (S. Pyo), heeyoung0908@chosun.ac.kr (H. Lee).

https://doi.org/10.1016/j.cscm.2024.e03691
Received 5 June 2024; Received in revised form 20 August 2024; Accepted 26 August 2024
Available online 28 August 2024

SWCNTs and examined microstructures using scanning electron microscopy (SEM) and transmission electron microscopy. The researchers discovered that the MWCNT solution could efficiently fill internal voids, unlike the SWCNT solution. Moreover, increasing the MWCNT content enhanced the thermal performance of the composite. Furthermore, producing SWCNTs is challenging and less cost-effective compared with that of MWCNTs. Accordingly, several studies have been conducted on cementitious composites that incorporate MWCNT solutions. Chaipanich et al. [15] analyzed the effects of incorporating MWCNTs and fly ash into cementitious composites, examining the influence on compressive strengths and microstructural characteristics of these materials. Appropriate amounts of MWCNT and fly ash improved the compressive strength of cementitious composites. Additionally, microstructural analysis revealed optimized material distribution and bonding conditions within the composites. Pop et al. [16] investigated the thermal conductivity of MWCNTs at room temperature and higher temperatures. Variations in the thermal conductivity of MWCNTs were observed concerning length and temperature conditions. Longer MWCNTs exhibited higher thermal conductivity, which decreased at excessively high temperatures.

The electrical properties of MWCNTs enable the detection of deformation and electrical resistance in cementitious composites in real time using sensors [17]. In addition, carbon is stable in extreme and highly corrosive environments, including acidic and alkaline conditions [18–21]. Choi et al. [22] dispersed MWCNTs using a magnetic field and added them to cementitious composites. Consequently, the thermal and electrical conductivity of the cementitious composites improved. Neitzert et al. [23] manufactured cementitious composites that integrate epoxy resin and MWCNTs, wherein the electrical resistance changes with temperature owing to the electrical properties of MWCNTs. This observation has led to the conclusion that MWCNTs can be used in heating systems. Lee et al. [24] added MWCNTs to cementitious composites and conducted thermal performance tests by varying the MWCNT content and number of curing days. The thermal performance of cementitious composites decreased as the number of curing days increased, but thermal conductivity increased as the MWCNT content increased. Cementitious composites incorporating MWCNTs have higher electrical and thermal performance than those incorporating other carbon fibers [25–33].

However, the influences of MWCNT on the mechanical properties of cementitious composites remain unclear. Kim et al. [34] synthesized cementitious composites by blending an MWCNT solution with silica fume. The addition of silica fume increased the compressive strength and filled the voids inside the cementitious composites. The study found that the compressive strength was reduced when the MWCNT content was $\geq$0.3 wt%. Goodarzi et al. [35] examined cementitious composites by dispersing MWCNTs using an upstream corrugated plate heat exchanger and analyzed the thermal performance and compressive strength. As the MWCNT content increased, the compressive strength decreased while the thermal performance increased. Xu et al. [36] synthesized cementitious composites by adding MWCNTs, and conducted compressive, bending, and tensile strength tests. The study found that the optimal MWCNT concentration was 0.2 % and that the mechanical properties had decreased owing to the agglomeration of the nanotubes caused by van der Waals forces when the optimal concentration was exceeded. Cheon et al. [37] developed MWCNT-anchored carbon fibers as a novel addition for carbon fiber reinforced thermoplastic polymers. Analyzing the compressive strength, the cementitious composite incorporating 1.0 wt% of MWCNT-anchored carbon fibers exhibited the highest compressive strength. The MWCNT-anchored carbon fibers formed an effective network with cement, consequently enhancing the thermal performance. The thermal performance of cementitious composites incorporating MWCNTs improves as the MWCNT content increases, but the compressive strength decreases when the added amount of MWCNTs exceeds the optimal owing to the agglomeration of the nanotubes caused by the van der Waals force. UHPC is a promising candidate used to mitigate the strength degradation of cementitious materials owing to its high durability [38–42]. UHPC demonstrates a compressive strength of $\geq$100 MPa when subjected to standard curing for 28 d and a compressive strength of $\geq$150 MPa when subjected to wet curing for 28 d.

UHPC requires the addition of silica fume, granulated blast furnace slag, and steel fibers in appropriate quantities [43–49]. Recent studies prepared cementitious composites using UHPC and analyzed various characteristics. Dawood et al. [50] studied cement mortar using hybrid fibers. The study analyzed the compressive strength according to the content of hybrid fibers in the UHPC mix. When the content of hybrid fibers in the mortar was 0.25 %, the compressive and bending strengths increased by 44 and 140 %, respectively. Salahaddin et al. [51] utilized recycled glass in the UHPC mix as a substitute for sand. The investigation classified particle sizes among various recycled glasses and validated recycled glass suitability based on compressive strength and bending strength tests. Ahmad et al. [52] conducted a compressive-strength test based on steel fiber content in UHPC. The compressive strength was increased by extending the curing period and steel fiber content but remained unaffected by the type of curing (heating and cooling cycles).

Conventional MWCNT cementitious composites have excellent thermal performance and electrical resistance, but their compressive strengths tend to decrease owing to the agglomeration of nanotubes caused by the van der Waals force [53–56]. This study aimed to confront these challenges by developing multifunctional MWCNT UHPC composites [57]. The multifunctional performance of the developed composites was examined by analyzing the power consumption and microstructures using compressive strength, thermal performance, and electrical resistance tests. In the compressive strength test, the MWCNT content and curing type were set as parameters. In addition, a digital image correlation system was used to analyze the crack modes of the MWCNT UHPC composites. In the thermal performance test, the MWCNT content, supply voltage, and number of curing days were set as parameters, and the thermal conductivity and heat generation of the fabricated cementitious composites were analyzed. The correlation between the thermal performance and power consumption of the MWCNT UHPC composites was obtained using an electrical resistance test. Regarding the microstructures of the MWCNT UHPC composites, the network between the MWCNT and UHPC particles was analyzed using field-emission scanning electron microscopy (FE-SEM). The thermal stability of the MWCNT UHPC composites according to the MWCNT content was tested using thermogravimetric analysis (TGA). In this analysis, the temperature range and chemical components of constituents of the MWCNT UHPC composites were identified, and thermal stability was evaluated. Finally, the effects of adding MWCNTs on the hydration reactions of the MWCNT UHPC composites were analyzed using X-ray diffraction (XRD).

2. Materials and methods

2.1. Materials

Table 1 presents the mixture proportions of the MWCNT UHPC composites. Silica, a strength additive, was used in fume and powder form with <10 % of the total weight. The water-to-cement ratio was fixed at 0.25. Cement and sand were mixed in a ratio of 1:1. A superplasticizer powder was used to secure the cement fluidity. The mixing ratio of both the silica fume and powder was 0.25. Silica fume was utilized to markedly enhance the strength and durability of concrete owing to its high pozzolanic reactivity. Furthermore, silica powder, despite being less reactive than fume, functioned as a physical filler, with the purpose of augmenting the internal density.

Table 2 summarizes the physical properties of the MWCNTs used in the experiment. The MWCNTs, which had an average diameter of 95 nm and an average length of 1.5 μm, were dispersed in a solution (instead of water) during the fabrication of the cementitious composites. Because the van der Waals forces causes the MWCNTs to agglomerate, the MWCNT solution was dispersed in a polyacrylic acid copolymer for 30 min using ultrasound at 22 kHz to ensure proper dispersion [58–60]. Ordinary Portland cement was used for the cement and quartz sand no. 20 for the sand, according to the American Society for Testing and Materials (ASTM) standards C 150 and C 778 [61,62]. In the thermal-performance test, electric current was supplied to the specimens through meshes. Because the use of steel fibers in cementitious composites would have made the thermal performance tests impossible owing to the electric current flow between meshes, steel fibers were excluded from the fabrication of the MWCNT UHPC composites.

Table 3 lists the parameters of the compressive strength test, namely the MWCNT content, curing type, and number of curing days. The MWCNT content was set to 0.125, 0.25, 0.5, and 1.0 wt%. The curing type was divided into room and high-temperature curing. The category “number of curing days” was divided into two classes (7 and 28 d). In total, 96 mortar specimens of MWCNT UHPC composites were prepared (with six specimens for each parameter). The specimens were named in the order of the MWCNT content, curing type, and number of curing days. For example, 0.125-R-7D indicates 0.125 wt% MWCNT UHPC composites subjected to room-temperature curing for 7 d.

Table 4 illustrates the parameters for the thermal performance test, namely the MWCNT content, number of curing days, and the voltage. The MWCNT content and number of curing days were identical to those of the compressive strength test. Room-temperature curing was used for the curing type. The voltage was set to 50, 100, 150, and 200 V. However, because of the safety concerns that may arise as strong electric currents flow via the bridge networks in the 1.0 wt% MWCNT specimens, the maximum voltage was set to 150 V for these specimens. In total, 72 mortar specimens were prepared, comprising three specimens for each parameter and supply voltage (50/100/150/200 V).

2.2. Fabrication

The MWCNT UHPC composites (size: 50 mm × 50 mm × 50 mm) were fabricated according to ASTM C 109 [63]. Fig. 1 shows the fabrication process of the MWCNT UHPC composite specimens. The first step involved the measurement and preparation of the materials, as shown in Fig. 1(a). The materials were then dry-mixed for 10 min to ensure they were well-mixed and consistent, as seen in Fig. 1(b). The MWCNT solution was then added to three separate batches of the mixture and mixed for 15 min (Fig. 1(c)). To maintain the cement fluidity, superplasticizer powder was added to the mixture. The three layers were then tamped 30 times each, as shown in Fig. 1(d). Finally, the specimens underwent room- and high-temperature curing. Room-temperature curing was performed for 7 and 28 d at 20 ± 2 °C. High-temperature curing was performed for 96 h at 90 °C and then for 7 and 28 d at 20 ± 2 °C (Fig. 1(e)(f)). In the thermal performance test, the specimens were named similarly to the compressive strength test, but the voltage was different for each parameter.

2.3. Experimental apparatus

Fig. 2 shows a conceptual diagram of the specimens used in the thermal performance test. Meshes were inserted into MWCNT UHPC composites after compacting the first layer to supply electricity. The mesh size was 2 mm, and the meshes were embedded at 20 and 5 mm intervals in the horizontal and vertical directions, respectively. A thermocouple was installed at the center of the specimen to measure the internal temperature of the cementitious composite.

The compressive strength test was performed using a universal testing machine (Fig. 3 (a)). The maximum capacity of the equipment was 1000 kN, with a loading rate set to 1 mm/min. In the thermal performance test, a power supply (ODA Technology, EX-200) and a data logger (TDS-540) were used. This test was conducted on a rubber plate for stability during voltage supply. The test was performed for 2 h until the maximum temperature. In the electrical resistance test, a digital multimeter (KEITHLEY, Model 2701) was used to analyze the correlation between the thermal performance and electrical resistance of the MWCNT UHPC composites. A

Table 1
Composition and ratios of multiwalled carbon nanotube ultrahigh-performance concrete (MWCNT UHPC) composites.

W/C (%)	Cement (g)	Sand (g)	Silica fume (g)	Silica powder (g)	Superplasticizer (g)
0.25	1000	1000	250	250	10

Table 2
Specific characterization of MWCNTs.

Property	Unit	Value	Measurement method
Average diameter	$10^{-9}m$	9.5	Transmission electron microscopy (TEM)
Average length	μm	1.5	TEM
Carbon purity	%	90	Thermogravimetric analysis
Transition metal oxide	%	<1 %	Inductively coupled plasma mass spectrometry
Surface area	m^2/g	250–300	Brunauer–Emmett–Teller surface area analysis
Volume resistivity	Ω·cm	10^{-9}	Internal test method (resistivity on powder)

Table 3
Parameters for compressive-strength test.

Specimen name	MWCNT content (wt%)	Curing type	Number of curing days (d)
0.125-R−7D	0.125	Room-temperature curing	7
0.125-R−28D			28
0.25-R−7D	0.25		7
0.25-R−28D			28
0.5-R−7D	0.5		7
0.5-R−28D			28
1.0-R−7D	1.0		7
1.0-R−28D			28
0.125-H−7D	0.125	High-temperature curing	7
0.125-H−28D			28
0.25-H−7D	0.25		7
0.25-H−28D			28
0.5-H−7D	0.5		7
0.5-H−28D			28
1.0-H−7D	1.0		7
1.0-H−28D			28

Table 4
Parameters for thermal performance test.

Specimen name	MWCNT content (wt%)	Number of curing days (d)	Voltage (V)
0.125-R−7D	0.125	7	100/150/200
0.125-R−28D		28	100/150/200
0.25-R−7D	0.25	7	100/150/200
0.25-R−28D		28	100/150/200
0.5-R−7D	0.5	7	100/150/200
0.5-R−28D		28	100/150/200
1.0-R−7D	1.0	7	50/100/150
1.0-R−28D		28	50/100/150

constant electric current was supplied to the two meshes installed in the specimen. As stated earlier, the MWCNT content and number of curing days were the test parameters. The measured electrical resistance of MWCNT UHPC composites and the supplied voltage were used to analyze the power consumption (Fig. 3(b)). The microstructures of the MWCNT UHPC composites were analyzed using FE-SEM. The equipment collected high-resolution images by generating electron rays using an FE gun. It analyzed the surface geometry, particle size and distribution, defects, and atypical structures. The analysis was based on the curing method and MWCNT content (Fig. 3(c)). In addition, the mass change under conditions during which the amount of heat supplied was constant was quantitatively analyzed using TGA. In the TGA, a constant temperature was applied to the tested specimen, and the corresponding mass was measured in real time. Arbitrarily selected samples (weight: 30 g) of the MWCNT UHPC composites were heated to 600 °C at a rate of 10 °C/min (Fig. 3(d)). Finally, the crystal structures of the specimens were analyzed using XRD. A few of the crystals caused the diffraction of rays. The diffraction angle and intensity are unique characteristics, thus offering insights into the structural composition and crystalline content within the specimen. Based on XRD analyses, the study investigated the effects of incorporating MWCNTs on the hydration reactions of MWCNT UHPC composites (Fig. 3(e)).

3. Results

3.1. Compressive strength

Fig. 4 illustrates the compressive strength test results for the MWCNT UHPC composites. High strengths of ≥80 MPa were measured at all MWCNT contents. The compressive strength of the 0.125-R specimen was 97.1 MPa at 7 d and 105.5 MPa at 28 d. The 0.25-R

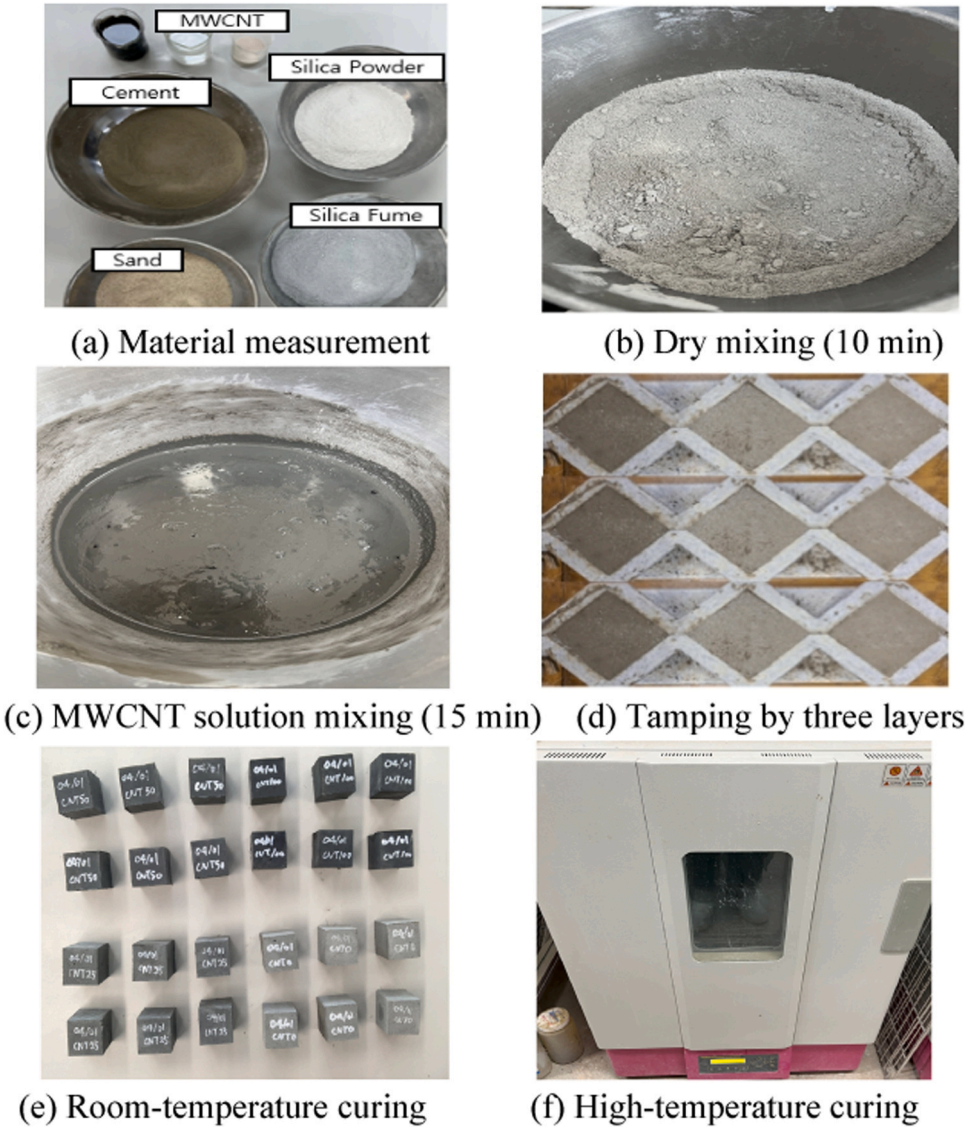

Fig. 1. Multiwalled carbon nanotube ultra-high-performance concrete (MWCNT UHPC) composite fabrication proces.

specimen exhibited a compressive strength of 107.1 MPa at 7 d and 114.7 MPa at 28 d, which was the highest in the group. The compressive strength of the 0.5-R specimen was 98.3 MPa at 7 d and 100.2 MPa at 28 d, while that of the 1.0-R specimen was 86.2 MPa at 7 d and 90.2 MPa at 28 d. Compared with the MWCNT content of 0.25 wt%, which had the highest compressive strength, the compressive strength decreased by 12 and 21 % when the MWCNT contents were 0.5 and 1.0 wt%, respectively (Fig. 4(a)). However, for the MWCNT UHPC composites subjected to high-temperature curing, the compressive strength increased for all MWCNT contents. The compressive strengths were 102.3 MPa at 7 d and 107.9 MPa at 28 d for the 0.125-H specimen, 115.8 MPa at 7 d and 120.8 MPa at 28 d for the 0.25-H specimen, 102.4 MPa at 7 d and 105.5 MPa at 28 d for the 0.5-H specimen, and 101.3 MPa at 7 d and 103.5 MPa at 28 d for the 1.0-H specimen. A maximum strength of 120.8 MPa was measured for the MWCNT content of 0.25 wt%, and the compressive strength decreased by 15 % when the MWCNT contents were 0.5 and 1.0 wt% (Fig. 4(b)). In contrast, for the 1.0-H specimen, the compressive strength reduction rate decreased owing to high-temperature curing. The MWCNT UHPC composites subjected to high-temperature curing generated calcium–silicate–hydrate (C–S–H) by accelerating the initial hydration reactions. The C–S–H addition effectively bolstered the compressive strength of the MWCNT UHPC composites by occupying internal voids, as evidenced by the microstructural analysis using FE-SEM.

Fig. 5 illustrates the analyzed cracks in the MWCNT UHPC composites during the compressive strength test using a digital image correlation system. For the 0.125-R-28D specimen, map cracks in the form of partial cracks were formed. Map cracks are cracks with irregular shapes. Uneven cracks appeared because the MWCNTs in the MWCNT UHPC composites disintegrated the connections between interfaces (Fig. 5(a)). The highest compressive strength was measured for the 0.25-R-28D specimen, which had complete

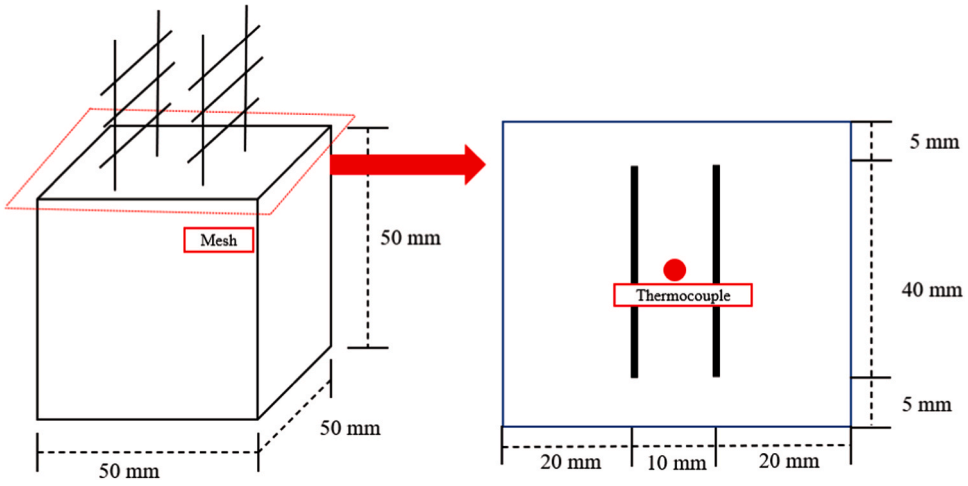

Fig. 2. Conceptual diagram of thermal performance experiment.

vertical cracks. Vertical cracks were observed in cementitious composites with the most uniform load distribution during loading. It was confirmed that the load distribution was uniform for the 0.25-R-28D specimen (Fig. 5(b)). The 0.5-R-28D specimen revealed vertical cracks only on one side. This could be attributed to the nonuniform distribution of the MWCNT particles (Fig. 5(c)). Separation cracks occurred in the 1.0-R-28D specimen; this specimen yielded the largest number of cracks and the lowest compressive strength (Fig. 5(d)).

3.2. *Thermal performance*

Table 5 lists the thermal performance results of the MWCNT UHPC composites according to the MWCNT content. When a voltage of 200 V was supplied, the temperature increased by 1.6 °C for the 0.125-R-7D specimen and by 1.1 °C for the 0.125-R-28D specimen. As 0.125 wt% MWCNT represents a sparse nanotube content, no temperature change occurred (Fig. 6(a)). At 200 V, the 0.25-R-7D specimen, with a heightened MWCNT content, exhibited a temperature increase of 15.1 °C compared with the 9.5 °C rise observed for the 0.25-R-28D specimen. An evident temperature change occurred for an MWCNT content of 0.25 wt% for the first time. The temperature increase was larger compared with that of the MWCNT content of 0.125 wt%, thus indicating that the thermal performance improves as the MWCNT content increases (Fig. 6(b)). At 200 V, the 0.5-R-28D specimen exhibited a temperature that was 31.3 °C less than that of the 0.5-R-7D specimen. The thermal performance of the MWCNT UHPC composites decreased as the number of curing days increased (Fig. 6(c)). The temperature of the 1.0-R-7D specimen increased by 70.6 °C when 150 V was supplied, while that of the 1.0-R-28D specimen, which completed the hydration reaction, increased by 40.7 °C. This indicates that an MWCNT content of 1.0 wt% can generate heat at high temperatures despite an increase in the number of curing days (Fig. 6(d)). The thermal performance of the MWCNT UHPC composites improved with an MWCNT content of 0.25 wt%. However, it decreased after 28 d when the hydration reactions were completed. This study discovered that the heating performance of the MWCNT UHPC composites became prominent with 0.25 wt% of MWCNT. MWCNTs have percolation thresholds for network formation [12,58]. Notably, the specimens with an MWCNT content of 0.125 wt% did not exhibit heating owing to the insufficient amount of MWCNT required for network formation. Meanwhile, the specimens with MWCNT contents $\geq$0.25 wt% generated heat owing to the optimal range of the percolation thresholds.

Fig. 7 illustrates the thermal images of the MWCNT UHPC composites when the maximum voltage was supplied. The MWCNT content was set as a parameter. The surface temperature of each specimen was measured in absolute terms, and imaging was performed for 2 h. The 0.125-R-7D and 0.125-R-28D specimens did not undergo significant heating as the surface temperatures were 20.9 and 20.1 °C, respectively (Fig. 7(a)(b)), because bridge networks were not formed in the microstructure owing to the insufficient MWCNT content. Owing to the higher MWCNT contents, the 0.25-R-7D and 0.25-R-28D specimens exhibited higher surface temperatures of 35.2 and 29.4 °C, respectively (Fig. 7(c)(d)). The surface temperature of the 0.5-R-7D specimen was 65.4 °C (Fig. 7(e)). Meanwhile, the surface temperature of the 0.5-R-28D specimen decreased to 33.7 °C (Fig. 7(f)). Thermal imaging revealed that this decrease occurred despite the application of the same voltage owing to the differences in the number of curing days. The MWCNT UHPC composites with MWCNT contents $\leq$0.5 wt% exhibited inhomogeneous temperature distributions owing to poor heat generation. Heating was concentrated in the top center part of the specimen with 0.25 wt% MWCNT and in the bottom center part of the specimen with 0.5 wt% MWCNT because electric current tends to flow along the shortest path.

Fig. 8 illustrates the thermal images of the 1.0-R-7D specimen at various voltages. The surface temperatures were 40.4 °C at 50 V (Fig. 8(a)) and 80.3 °C at 100 V (Fig. 8(b)). At a maximum voltage of 150 V, it increased to as high as 90.6 °C (Fig. 8(c)). The 1.0-R-7D specimen exhibited a relatively uniform temperature distribution compared with that of the 0.125-R-7D specimen. The temperature distributions of the MWCNT UHPC composites were uniform at an MWCNT content of 1.0 wt%.

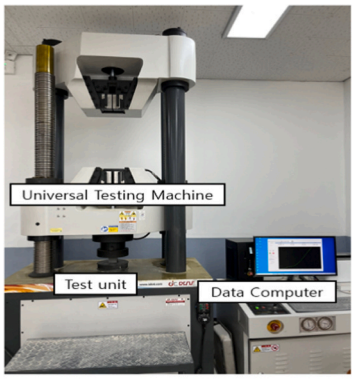

(a) Universal testing machine

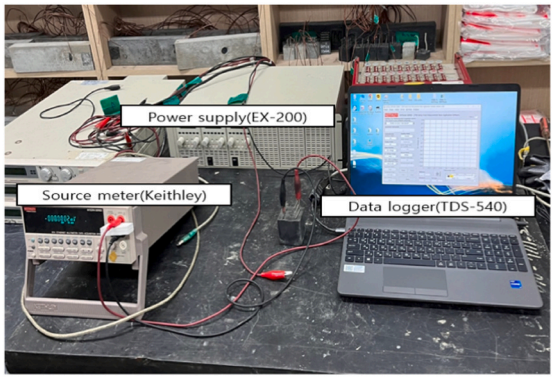

(b) Thermal performance and electrical resistance tests

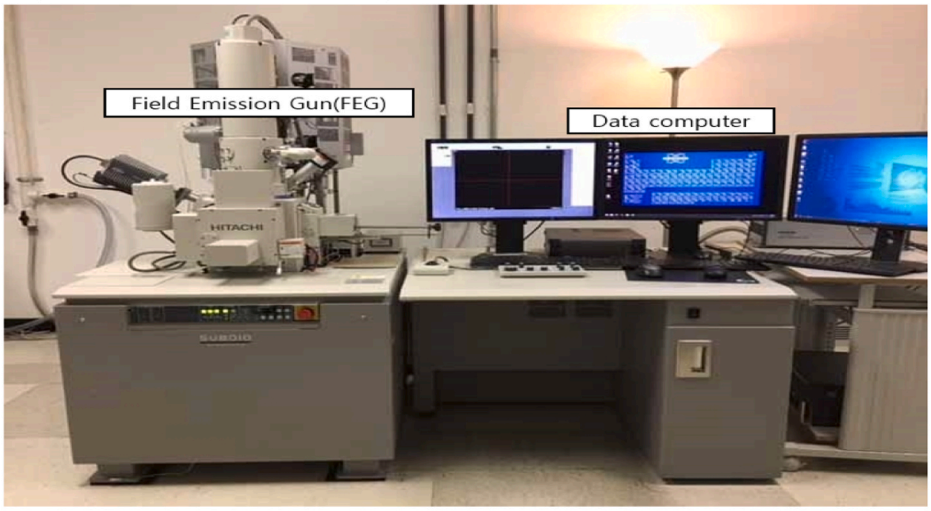

(c) Field-emission scanning electron microscopy test

(d) Thermogravimetric analysis

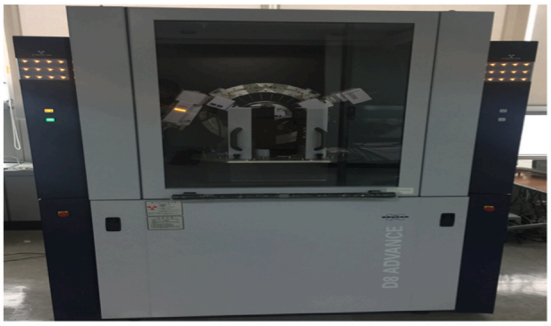

(e) Multipurpose X-ray diffractometer test

Fig. 3. Setup of thermal, electrical, and mechanical performance experiments.

3.3. Electrical resistance

Fig. 9 depicts the relationship between the electrical resistance of the MWCNT UHPC composites and the number of curing days. The electrical resistance was measured at 3, 8, 12, 22, and 28 d. On the 28th day of curing, the specimens containing 0.125 wt% MWCNT exhibited the highest electrical resistance of 117.35 kΩ, while those with 1.0 wt% MWCNT demonstrated the lowest, at 0.18 kΩ. The electrical resistance of the 0.25 wt% MWCNT specimen was 3.91 kΩ higher at 28 d than at 3 d, whereas the 0.5 wt% MWCNT specimen exhibited a resistance difference of 0.49 kΩ between 3 and 28 d. The electrical resistance of the MWCNT UHPC composites increased as the number of curing days increased; this was because the moisture content in the specimen decreased owing to the completion of the hydration reactions. When the MWCNT content was 0.125 wt%, a higher resistance was observed owing to the absence of MWCNT bridge networks, reducing the thermal performance.

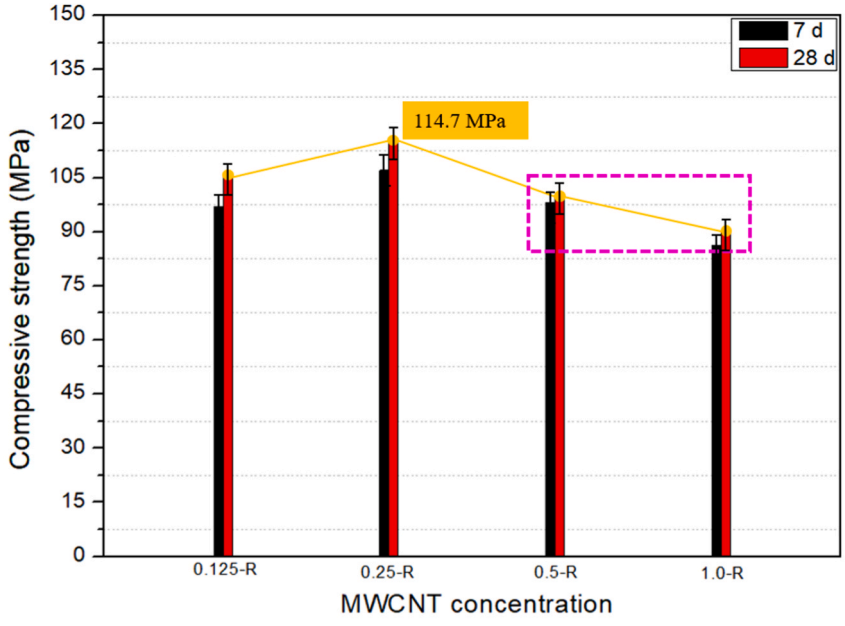

(a) Room-temperature curing of MWCNT UHCPC composites

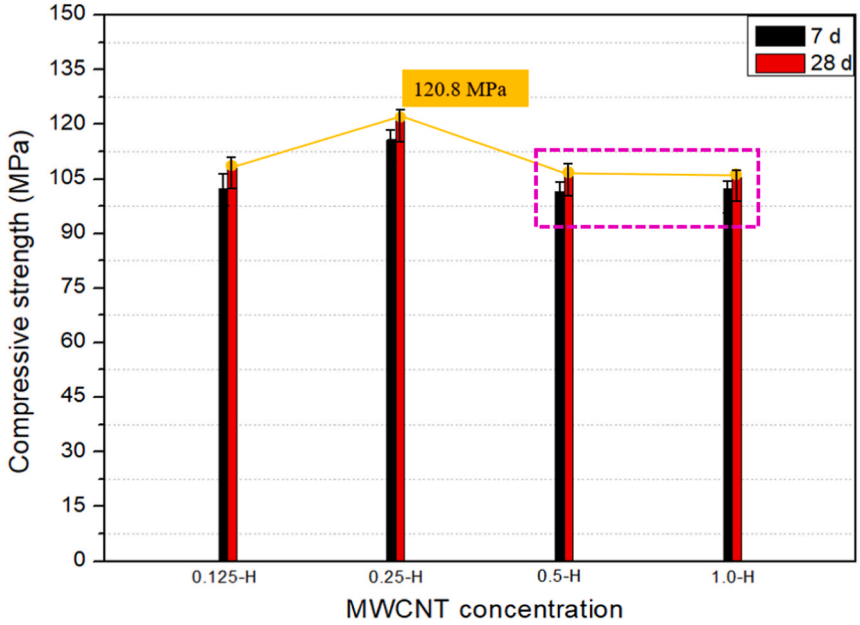

(b) High-temperature curing of MWCNT UHCPC composites

Fig. 4. Compressive strength results according to MWCNT mixing concentration.

The power consumption was calculated using the relationships between the voltage and current or between the voltage and electrical resistance. Table 6 lists the power consumption results (for each parameter) obtained using Eq. (1) when the maximum voltage was applied.

$$P = V \times I = \frac{V^2}{R}, \tag{1}$$

where P is the power consumption, V is the voltage, I is the current, and R is the electrical resistance. The units of power, voltage, current, and resistance were W, V, A, and Ω, respectively. Therefore, power consumption can be derived using the voltage and

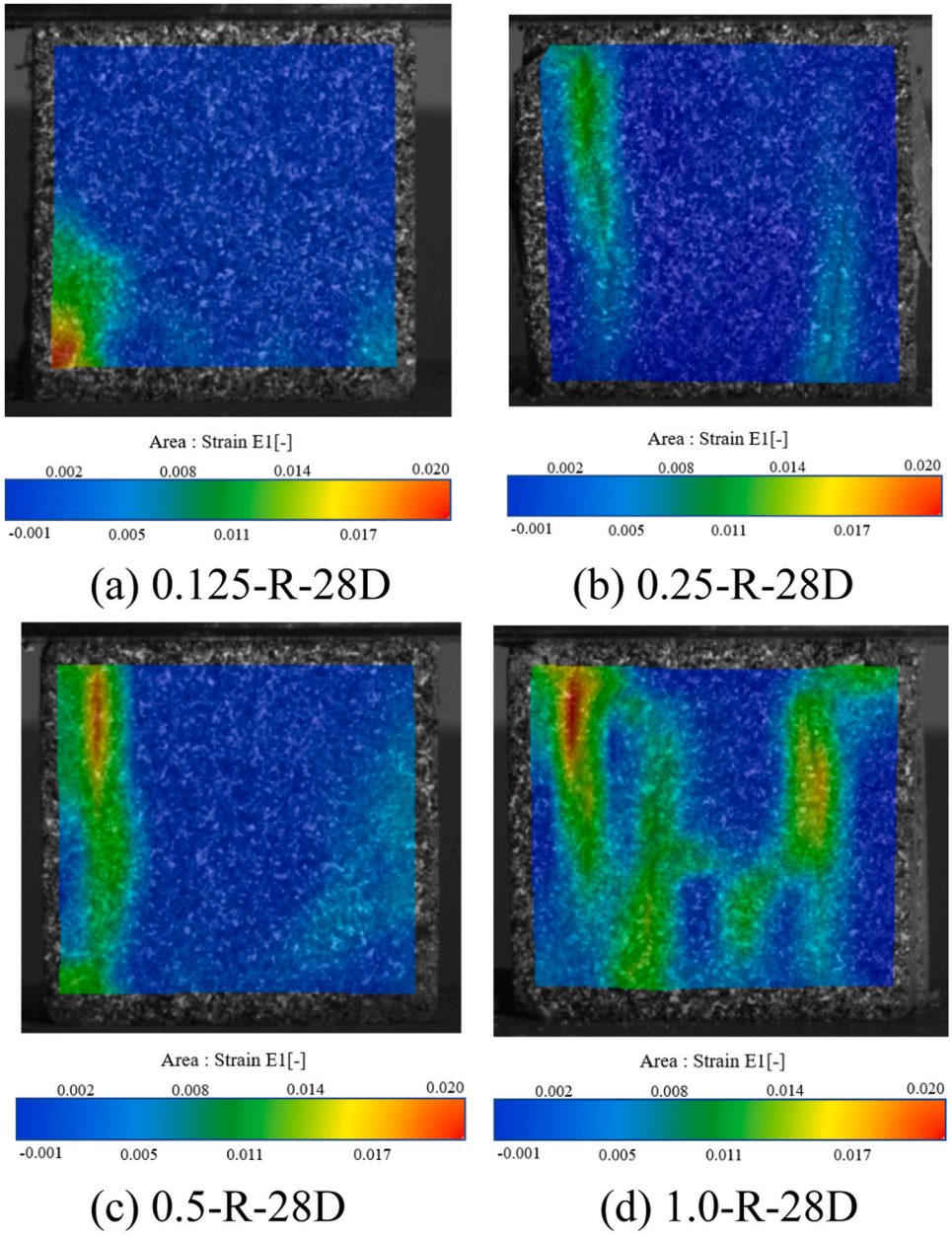

Fig. 5. Digital image correlation outcomes following crack analysis for MWCNT UHPC composites.

electrical resistance values obtained from the experiment based on the ratio $\frac{V^2}{R}$. The 0.125 wt% MWCNT specimen demonstrated the lowest power consumption with a decrease of approximately 13 W after 28 d. Initially, the power consumption was 427.17 W and declined to 410.04 W over time. Conversely, the 0.5 wt% MWCNT specimen consumed 20.20 kW, which was approximately five times higher than that consumed by the 0.25 wt% MWCNT specimen. In contrast, the 1.0 wt% MWCNT specimen exhibited the highest power consumption, initiating at 562.50 kW, with a subsequent reduction of approximately 430 W after 28 d. This can be attributed to the improved electrical conductivity and heating performance due to the addition of 1.0 wt% MWCNT to the cementitious composites. Power consumption in the MWCNT UHPC composites increased proportionally with the MWCNT content and decreased as a function of the curing period.

Power consumption of the MWCNT UHPC composites increased as a function of the MWCNT content and curing period. For example, after 3 d of curing, the power consumption of the 0.5 wt% MWCNT specimen increased by 17.13 W compared with the consumption at 28 d. Similarly, the power consumption of the 1.0 wt% MWCNT specimen increased by 437.5 W after 3 d compared with the consumption at 28 d. Notably, the power consumption of the 1.0 wt% MWCNT UHPC specimen decreases significantly

Table 5
Thermal performance of MWCNT UHPC composites.

Specimen	Voltage (V)	Thermal performance (°C)
0.125-R−7D	100	1.4
	150	1.6
	200	1.6
0.125-R−28D	100	0.5
	150	0.9
	200	1.1
0.25-R−7D	100	5.7
	150	9.3
	200	15.1
0.25-R−28D	100	3.8
	150	7.2
	200	9.5
0.5-R−7D	100	8.3
	150	10.0
	200	45.0
0.5-R−28D	100	2.5
	150	4.2
	200	13.7
1.0-R−7D	50	20.5
	100	60.9
	150	70.6
1.0-R−28D	50	10.5
	100	30.5
	150	40.7

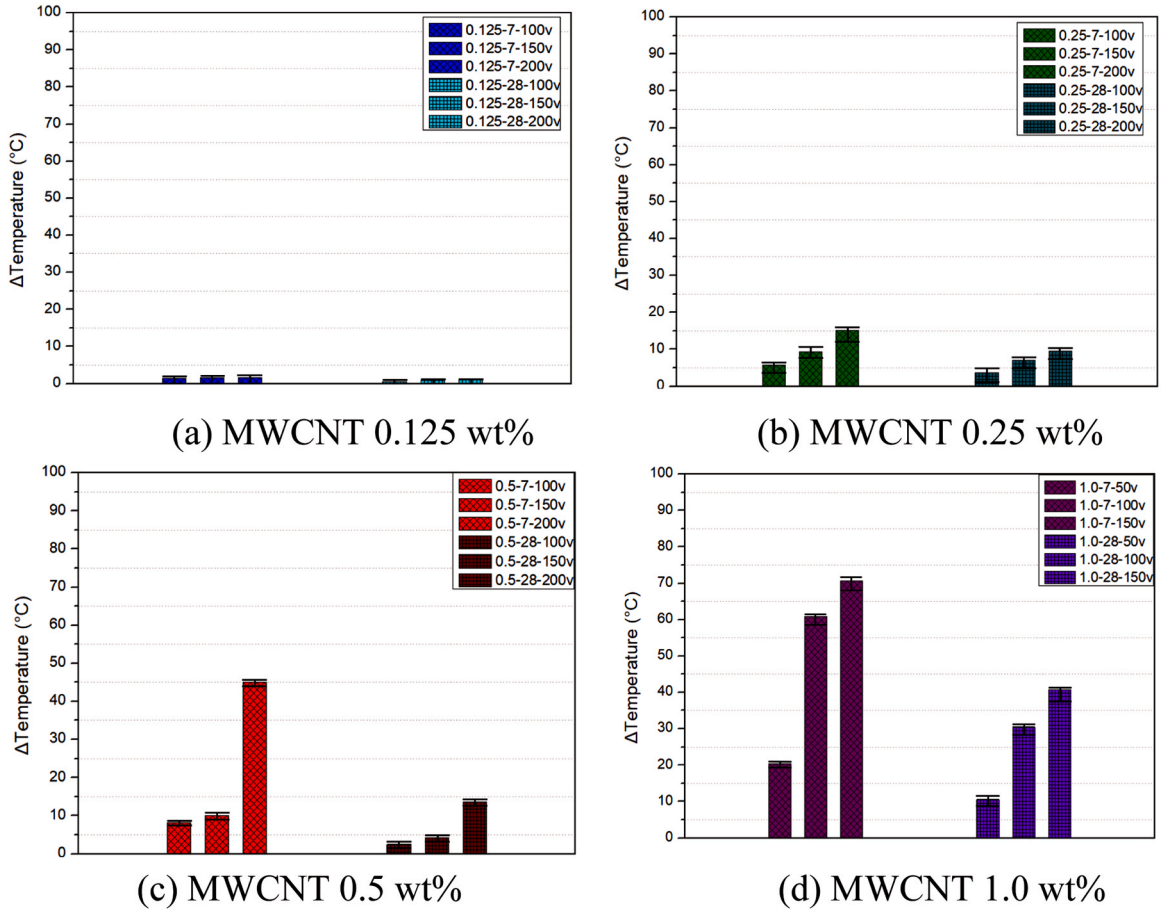

Fig. 6. Temperature variations in MWCNT UHPC composites.

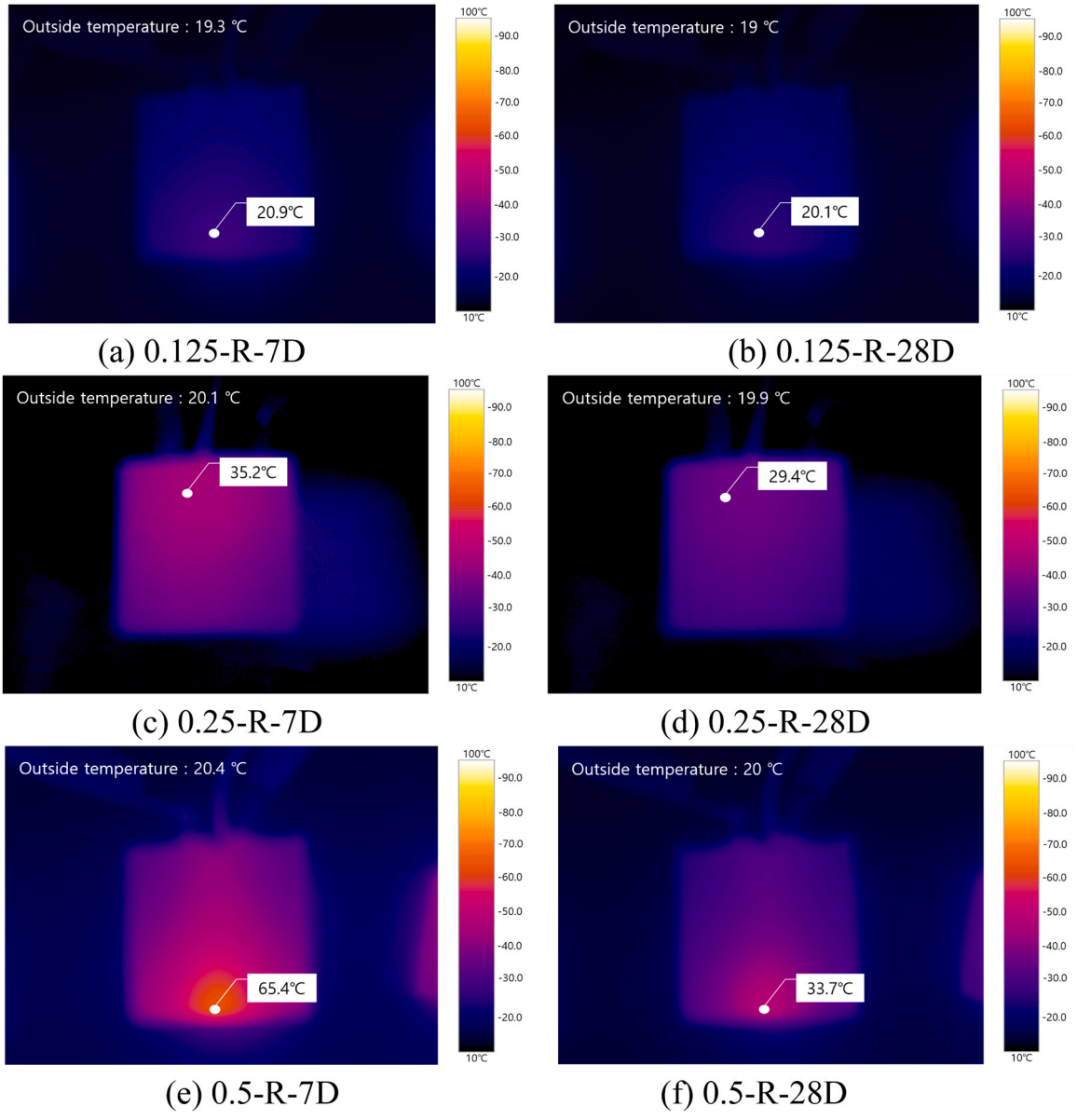

Fig. 7. Thermal imaging of MWCNT UHPC composites at various MWCNT concentrations.

depending on the curing duration relative to the other mixing concentrations. These results imply a linear relationship between the MWCNT concentration and power consumption.

3.4. Microstructural analysis

Fig. 10 shows the analyzed FE-SEM results for the MWCNT UHPC composites according to the curing type. The red crosses in the figure indicate MWCNTs and the yellow crosses are C–S–H. For both the 1.0-R-28D and 1.0-H-28D specimens, several agglomerations were observed owing to the van der Waals forces among the MWCNT particles. These MWCNT agglomerations were the main cause of the degraded compressive strength at an MWCNT content in the range of 0.5–1.0 wt%. However, the 1.0-H-28D specimen generated more C–S–H than the 1.0-R-28D specimen because initial hydration reactions were accelerated by high-temperature curing. To conclude, this phenomenon reduced the reduction rate of the compressive strength because the generated C–S–H filled the interstitial voids inside the cementitious composites. In addition, it was confirmed that the increased composite strength due to the increased MWCNT content was comparable to the nanoparticle effect[64,65].

Fig. 11 depicts the FE-SEM analysis results for the MWCNT UHPC composites according to the MWCNT content. For the 0.125-R-28D specimen, which had the lowest MWCNT content, the MWCNT particles did not agglomerate; in contrast, the 1.0-R-28D specimen,

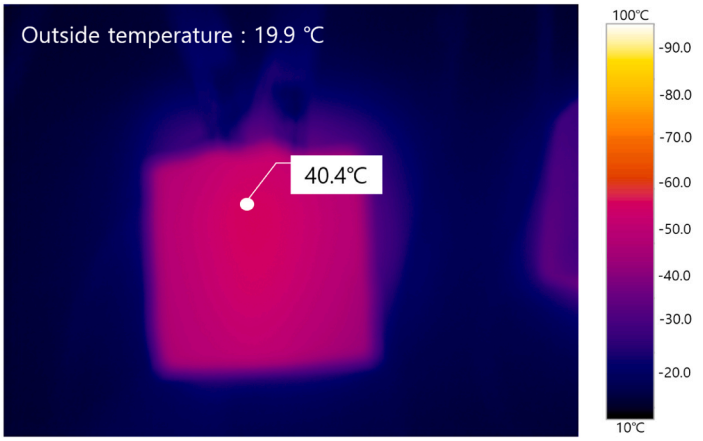

(a) 50 V

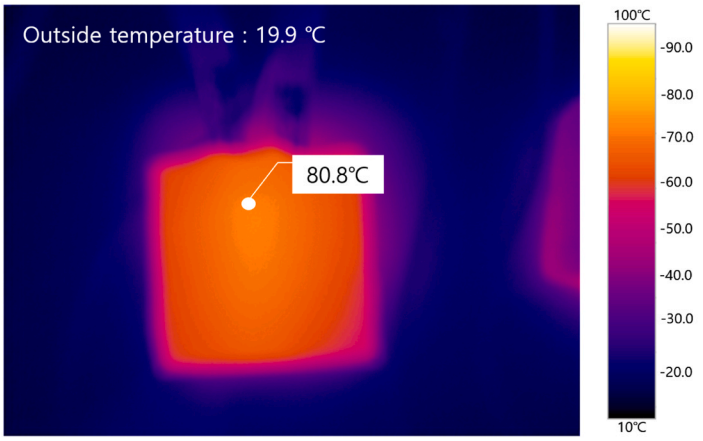

(b) 100 V

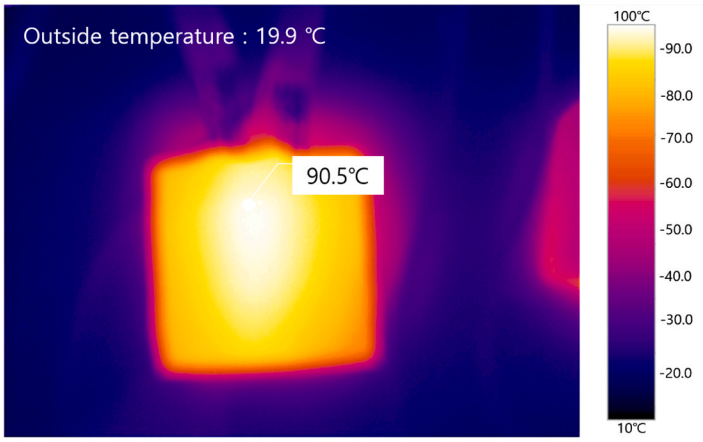

(c) 150 V

Fig. 8. Thermal imaging of 1.0 wt% MWCNT UHPC composites according to voltage.

which had the highest MWCNT content, exhibited several newly formed MWCNT bridge networks. These networks between the MWCNT particles were not formed in the 0.125-R-28D specimen owing to the low MWCNT content. Owing to the elevated MWCNT content, the 1.0-R-28D specimen formed networks that enhanced the thermal performance by linking the microstructures of the cementitious composite.

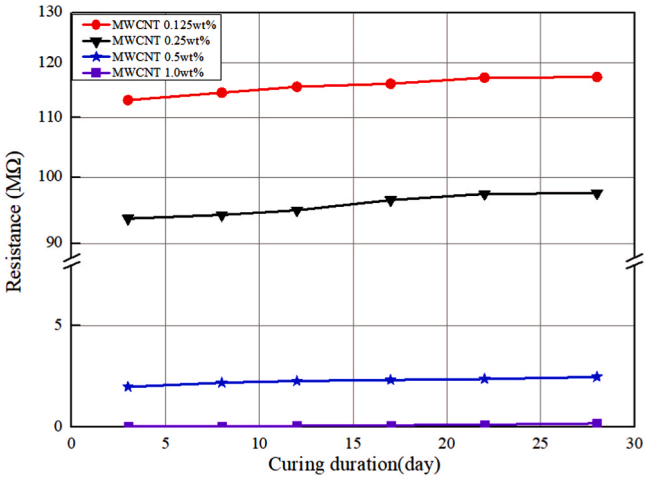

Fig. 9. Electrical resistance of MWCNT UHPC composites according to curing duration.

Table 6
Electrical resistances of MWCNT UHPC composites at different curing periods.

Specimen	Curing period (d)	Voltage (V)	Electrical resistance (kΩ)	Power consumption (W)
0.125 wt% MWCNT	3	200 V	113.13	353.57
	8		114.47	349.44
	12		115.54	346.20
	17		116.12.	344.47
	22		117.23	341.21
	28		117.35	340.86
0.25 wt% MWCNT	3	200 V	93.64	427.17
	8		94.21	424.58
	12		94.92	421.41
	17		96.47	414.64
	22		97.43	410.55
	28		97.55	410.04
0.5 wt% MWCNT	3	200 V	1.98	20.20×10^3 18.26×10^3 17.62×10^3 17.24×10^3 16.87×10^3 16.19×10^3
	8		2.19	
	12		2.27	
	17		2.32	
	22		2.37	
	28		2.47	
1.0 wt% MWCNT	3	150 V	0.04	562.50×10^3 562.50×10^3 375.00×10^3 250.00×10^3 187.50×10^3 125.00×10^3
	8		0.04	
	12		0.06	
	17		0.09	
	22		0.12	
	28		0.18	

Fig. 12 illustrates the TGA curves of the MWCNT UHPC composites according to the MWCNT content. The weight ratio rapidly decreases when the temperature is in the range of 100–200 °C for all four weight percentages. It is posited that $Ca(OH)_2$ was decomposed by dehydration in this temperature range. The weight ratios were found to be similar (approximately 93.5 %) for specimens with MWCNT contents of ≥0.25 wt%. However, an MWCNT content of 0.125 wt% exhibited a marginally higher weight ratio (94.5 %) than an MWNCT content of 1.0 wt%. These results confirm the thermal stability observed at an MWCNT content of 0.125 wt%, which effectively prevents heating.

Fig. 13 illustrates the XRD analysis results for four MWCNT UHPC composite specimens. In the experiment, the MWCNT content was set as a parameter. The incident and reflection angles of the X-rays were considered. For the four specimens, $Ca(OH)_2$ was observed at $2\theta = 20°–21°$, Carbon was observed at $2\theta = 29°–30°$, $CaCO_3$ was observed at $2\theta = 42°–43°$, Silica (SiO_2) appeared at $2\theta = 49°–50°$, and C–S–H, a hydration product, was detected at $2\theta = 68°–69°$. The XRD analysis results, expressed in arbitrary units (a.u.), showed that the XRD patterns of the MWCNT UHPC composites were similar even though they contained different MWCNT contents. Therefore, the hydrates of the specimens were unaffected when the MWCNT content was in the range of 0.125–1.0 wt%. Additionally, the interfacial transition zone (ITZ) between the MWCNTs and cement matrix was analyzed, revealing no significant changes in composition across different MWCNT contents, indicating a stable ITZ regardless of the MWCNT content[66,67]. If needed, the

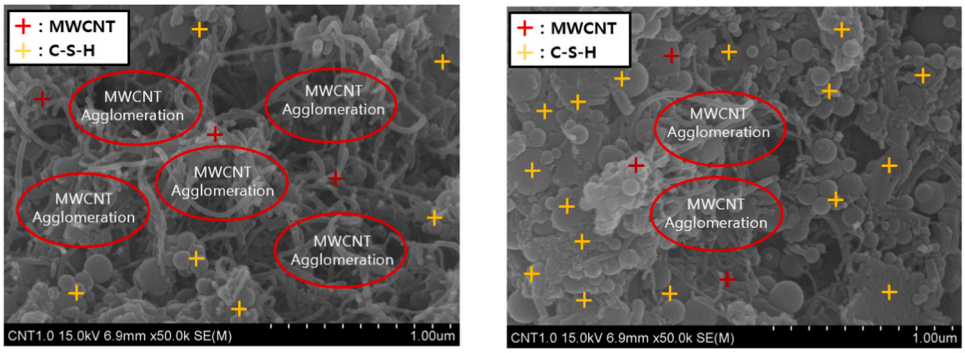

(a) 1.0-R-28D (b) 1.0-H-28D

Fig. 10. Field-emission scanning electron microscopy (FE-SEM) of MWCNT UHPC composites cured with different curing methods.

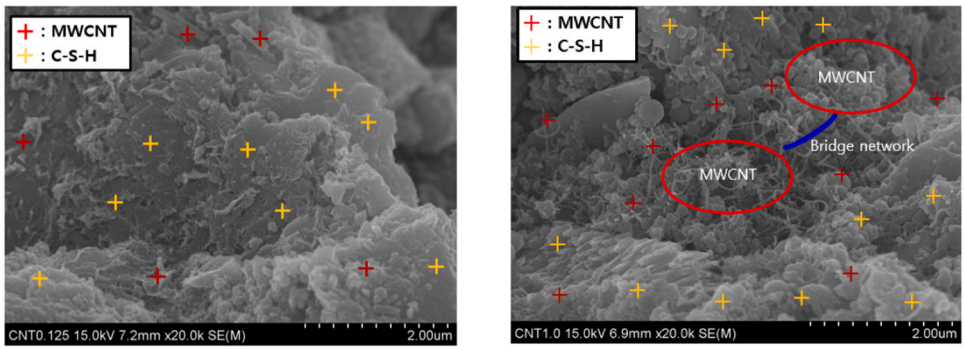

(a) 0.125-R-28D (b) 1.0-R-28D

Fig. 11. FE-SEM of MWCNT UHPC composite according to MWCNT concentration.

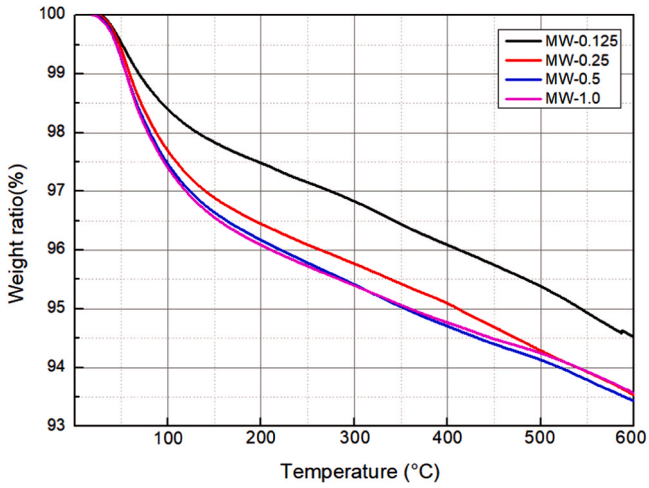

Fig. 12. Thermogravimetric curves of MWCNT UHPC composites.

intensity could also be represented as 'count' based on the preference or convention used.

4. Conclusions

In this study, compressive strength, thermal performance, and electrical resistance tests were conducted to examine the

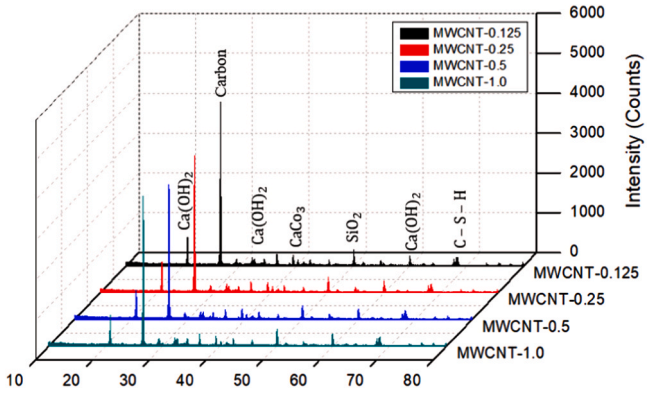

Fig. 13. X-ray diffraction patterns of MWCNT UHPC composites.

multifunctional performance of MWCNT UHPC composites. The microstructures of the MWCNT UHPC composites were analyzed using FE-SEM, TGA, and XRD. Based on the experiment results of this study, the following conclusions were drawn.

1. The compressive strength of all MWCNT UHPC composites (except 0.25-R-28D) decreased when the MWCNT content was ≥0.5 wt % owing to the agglomeration of MWCNT particles caused by the interparticle van der Waals force. Meanwhile, the 0.25-R-28D specimen exhibited a high-compressive strength of 114.7 MPa. The 0.25 wt% MWCNT UHPC composites yielded the highest compressive strength. The FE-SEM analysis results showed that the compressive strength of the specimens containing a MWCNT content in the range of 0.5–1.0 wt% decreased owing to several agglomerations caused by the van der Waals force between MWCNT particles. Hence, the correct MWCNT content should be added to obtain a relatively high-compressive strength for MWCNT UHPC composites.
2. In the thermal performance test of the MWCNT UHPC composites, specimens with MWCNT contents of 0.125 wt% exhibited almost no temperature change and the temperature variation of specimens with MWCNT contents of 1.0 wt% increased by up to 70.6 °C. As percolation thresholds for network formation appeared at MWCNT contents of ≥0.25 wt%, specimens with MWCNT contents of 0.125 wt% did not display heating performance. The FE-SEM analysis results of the MWCNT UHPC composites based on the MWCNT content showed that no bridge network was formed when the MWCNT content was 0.125 wt% owing to the low MWCNT content. However, the 1.0 wt% MWCNT UHPC composites contained several bridge networks. The MWCNT bridge networks improved thermal performance by acting as internal electrical connections within the MWCNT UHPC composites.
3. The electrical resistance test results confirmed that the electrical resistance of the MWCNT UHPC composites increased. Additionally, the thermal performance decreased with the number of curing days. The power consumption of the MWCNT UHPC composites decreased as the curing period increased. The desired power consumption of the MWCNT UHPC composites can be derived from the number of curing days.
4. The TGA analysis results based on the MWCNT content showed that specimens with MWCNT contents of 0.125 wt% showed a marginally higher weight ratio (94.5 %) than other MWCNT concentrations. This led to the conclusion that MWCNT UHPC composites exhibited poor heating performance at MWCNTs contents of ≤0.125 wt% owing to the high-thermal stability. In future studies, the addition of new admixtures to enhance the thermal conductivity of 0.125 wt% MWCNT UHPC composites should be explored. The XRD analysis results indicated no notable distinction between the hydrates of 0.125 wt% MWCNT and those of 1.0 wt % MWCNT for the MWCNT UHPC composites. Thus, the MWCNTs and cement hydrates did not react with each other. These hydrates, generated via hydration reactions in the MWCNT UHPC composites, remained unaffected by the MWCNT content.
5. MWCNT UHPC composites can be created with a maximum ultrahigh strength of 120.8 MPa. The addition of MWCNTs enabled heating to a maximum surface temperature of 90.6 °C. The power consumption of MWCNT UHPC composites can also be predicted from the type of curing and the number of curing days. Therefore, MWCNT UHPC composites can be used in various applications in the field of civil engineering as new construction materials with excellent strength, heating, and electrical performance.

Ethics approval and consent to participate

Not applicable.

Data statement

The data and materials are included in the manuscript.

CRediT authorship contribution statement

Heeyoung Lee: Writing – review & editing, Writing – original draft, Project administration. **Sunho Kang:** Writing – original draft,

Investigation, Formal analysis, Conceptualization. **Sukhoon Pyo:** Writing – review & editing, Writing – original draft.

Declaration of Competing Interest

The authors declare that they have no known competing financial interests or personal relationships that could have appeared to influence the work reported in this paper.

Data availability

Data will be made available on request.

Acknowledgments

This research work was supported by the Basic Science Research Program [grant number 2020R1C1C1005448] and the Regional Innovation Strategy (RIS) [grant number 2021RIS-002] through the National Research Foundation of Korea (NRF), funded by the Ministry of Education (MOE).

Consent for publication

Not applicable.

References

[1] H. Li, Y. Li, C. Jin, The energy dissipation property of MWCNTs cement paste composites, Constr. Build. Mater. 327 (2022) 126953, https://doi.org/10.1016/j.conbuildmat.2022.126953.
[2] F. Yu, T. Sun, S. Dong, S. Ding, B. Han, Chloride penetration resistance of ultra-high-performance concrete with various multi-walled carbon nanotubes, Constr. Build. Mater. 421 (2024) 135751, https://doi.org/10.1016/j.conbuildmat.2024.135751.
[3] B. Kan, N. Anand, E. Lubloy, D. Andrushia, Influence of multi-walled carbon nanotube (MWCNT) on flexural behavior and microstructure characteristics of geopolymer concrete beams, Case Stud. Constr. Mater. (2024) e03317, https://doi.org/10.1016/j.cscm.2024.e03317.
[4] C. Jongvivatsakul, A. Thongchom, T. Mathuros, T. Prasertsri, M. Adamu, S. Orasutthikul, T. Charainpanitkul, Enhancing bonding behavior between carbon fiber-reinforced polymer plates and concrete using carbon nanotube reinforced epoxy composites, Case Stud. Constr. Mater. 17 (2022) e01407, https://doi.org/10.1016/j.cscm.2022.e01407.
[5] A. Dul, T. Salet, S. Oliveira, A study of the effects of MWCNTs on the fresh and hardened state properties of 3D printable concrete, Case Stud. Constr. Mater. 20 (2024) e02913, https://doi.org/10.1016/j.cscm.2024.e02913.
[6] S. Ding, Y. Xiang, Y. Ni, K. Thakur, X. Wang, B. Han, J. Ou, In-situ synthesizing carbon nanotubes on cement to develop self-sensing cementitious composites for smart high-speed rail infrastructures, Nano Today 43 (2022) 101438, https://doi.org/10.1016/j.nantod.2022.101438.
[7] S. Ding, X. Wang, L. Qiu, Q. Ni, X. Dong, Y. Cui, J. Ou, Self-sensing cementitious composites with hierarchical carbon fiber-carbon nanotube composite fillers for crack development monitoring of a maglev girder, Small 19 (9) (2023) 2206258, https://doi.org/10.1002/smll.202206258.
[8] H. Allujami, M. Abdulkareem, M. Jassam, T. M, R. Al-Mansob, A. Ibrahim, L. Ng, C. Yam, Mechanical properties of concrete containing recycle concrete aggregates and multi-walled carbon nanotubes under static and dynamic stresses, Case Stud. Constr. Mater. 17 (2022) e01651, https://doi.org/10.1016/j.cscm.2022.e01651.
[9] H. Lee, W. Yu, L. Kj, W. Chung, Self-heating and electrical performance of carbon nanotube-enhanced cement composites, Constr. Build. Mater. 250 (2020) 118838, https://doi.org/10.1016/j.conbuildmat.2020.118838.
[10] S. Chuah, Z. Pan, J.G. Sanjayan, C.M. Wang, W.H. Duan, Nano reinforced cement and concrete composites and new perspective from graphene oxide, Constr. Build. Mater. 73 (2014) 113–124, https://doi.org/10.1016/j.conbuildmat.2014.09.040.
[11] M.S. Konsta-Gdoutos, Z.S. Metaxa, S.P. Shah, Highly dispersed carbon nanotube reinforced cement based materials, Cem. Concr. Res. 40 (7) (2010) 1052–1059, https://doi.org/10.1016/j.cemconres.2010.02.015.
[12] M.S. Konsta-Gdoutos, Z.S. Metaxa, S.P. Shah, Multi-scale mechanical and fracture characteristics and early-age strain capacity of high performance carbon nanotube/cement nanocomposites, Cem. Concr. Compos. 32 (2) (2010) 110–115, https://doi.org/10.1016/j.cemconcomp.2009.10.007.
[13] B. Mahanthesh, B.J. Gireesha, I.L. Animasaun, T. Muhammad, N.S. Shashikumar, MHD flow of SWCNT and MWCNT nanoliquids past a rotating stretchable disk with thermal and exponential space dependent heat source, Phys. Scr. 94 (8) (2019) 085214, https://doi.org/10.1088/1402-4896/ab18ba.
[14] H. Lee, D. Kang, J. Kim, K. Choi, W. Chung, Void detection of cementitious grout composite using single-walled and multi-walled carbon nanotubes, Cem. Concr. Compos. 95 (2019) 237–246, https://doi.org/10.1016/j.cemconcomp.2018.10.003.
[15] A. Chaipanich, T. Nochaiya, W. Wongkeo, P. Torkittikul, Compressive strength and microstructure of carbon nanotubes–fly ash cement composites, Mater. Sci. Eng. A 527 (4–5) (2010) 1063–1067, https://doi.org/10.1016/j.msea.2009.09.039.
[16] E. Pop, D. Mann, Q. Wang, K. Goodson, H. Dai, Thermal conductance of an individual single-wall carbon nanotube above room temperature, Nano Lett. 6 (1) (2006) 96–100, https://doi.org/10.1021/nl052145f.
[17] X. Yu, E. Kwon, A carbon nanotube/cement composite with piezoresistive properties, Smart Mater. Struct. 18 (5) (2009) 055010, https://doi.org/10.1088/0964-1726/18/5/055010.
[18] H.K. Kim, Chloride penetration monitoring in reinforced concrete structure using carbon nanotube/cement composite, Constr. Build. Mater. 96 (2015) 29–36, https://doi.org/10.1016/j.conbuildmat.2015.07.190.
[19] H. Lee, S. Jeong, W. Chung, Enhancing bond performance: carbon fiber reinforced polymer bar interaction with multi-walled carbon nanotubes cementitious composites in chloride-exposed conditions, Constr. Build. Mater. 412 (2024) 134763, https://doi.org/10.1016/j.conbuildmat.2023.134763.
[20] M.D.C. Camacho, O. Galao, F.J. Baeza, E. Zornoza, P. Garcés, Mechanical properties and durability of CNT cement composites, Materials 7 (3) (2014) 1640–1651, https://doi.org/10.3390/ma7031640.
[21] H. Lee, S. Park, S. Cho, W. Chung, Correlation analysis of heating performance and electrical energy of multi-walled carbon nanotubes cementitious composites at sub-zero temperatures, Compos. Struct. 238 (2020) 111977, https://doi.org/10.1016/j.compstruct.2020.111977.
[22] E.S. Choi, J.S. Brooks, D.L. Eaton, M.S. Al-Haik, M.Y. Hussaini, H. Garmestani, D. Li, K. Dahmen, Enhancement of thermal and electrical properties of carbon nanotube polymer composites by magnetic field processing, J. Appl. Phys. 94 (9) (2003) 6034–6039, https://doi.org/10.1063/1.1616638.
[23] H.C. Neitzert, L. Vertuccio, A. Sorrentino, Epoxy/MWCNT composite as temperature sensor and electrical heating element, IEEE Trans. Nanotechnol. 10 (4) (2010) 688–693, https://doi.org/10.1109/TNANO.2010.2068307.

[24] H. Lee, J. Seong, W. Chung, Effect of curing time on thermal response characterization of carbon-nano cementitious composites, Compos. Struct. 265 (2021) 113781, https://doi.org/10.1016/j.compstruct.2021.113781.
[25] C. Gao, L. Huang, L. Yan, R. Jin, H. Chen, Mechanical properties of recycled aggregate concrete modified by nano-particles, Constr. Build. Mater. 241 (2020) 118030, https://doi.org/10.1016/j.conbuildmat.2020.118030.
[26] H. Lee, S. Jeong, S. Cho, W. Chung, Enhanced bonding behavior of multi-walled carbon nanotube cementitious composites and reinforcing bars, Compos. Struct. 243 (2020) 112201, https://doi.org/10.1016/j.compstruct.2020.112201.
[27] R. Hamzaoui, A. Bennabi, S. Guessasma, R. Khelifa, N. Leklou, Optimal carbon nanotubes concentration incorporated in mortar and concrete, Adv. Mater. Res. 587 (2012) 107–110, https://doi.org/10.4028/www.scientific.net/AMR.587.107.
[28] H. Lee, S. Park, D. Kim, W. Chung, Heating performance of cementitious composites with carbon-based nanomaterials, Crystals 12 (2022) 716, https://doi.org/10.3390/cryst12050716.
[29] T. Yahyae, S. Mofidi, The impact of multi-walled carbon nanotubes on the mechanical and environmental properties of porous concrete in removing pollutants for use in surface runoffs, e02697, Case Stud. Constr. Mater. 20 (2024), https://doi.org/10.1016/j.cscm.2023.e02697.
[30] S. Eisa, A. Mohamady, M. Basiouny, A. Abdulhamid, R. Kim, Mechanical properties of asphalt concrete modified with carbon nanotubes (CNTs), Case Stud. Constr. Mater. 16 (2022) e00930, https://doi.org/10.1016/j.cscm.2022.e00930.
[31] H. Lee, W. Yu, W. Chung, Damage detection of carbon nanotube cementitious composites using the thermal and electrical resistance properties, Appl. Sci. 11 (2021) 2955, https://doi.org/10.3390/app11072955.
[32] S.T. Kang, S.H. Park, Experimental study on improving compressive strength of MWCNT reinforced cementitious composites, J. Kor. Concr. Inst. 26 (1) (2014) 63–70, https://doi.org/10.4334/JKCI.2014.26.1.063.
[33] S. Kumar, P. Kolay, S. Malla, S. Mishra, Effect of multiwalled carbon nanotubes on mechanical strength of cement paste, J. Mater. Civ. Eng. 24 (1) (2012) 84–91, https://doi.org/10.1061/(ASCE)MT.1943-5533.0000350.
[34] H.K. Kim, I.W. Nam, H.K. Lee, Enhanced effect of carbon nanotube on mechanical and electrical properties of cement composites by incorporation of silica fume, Compos. Struct. 107 (2014) 60–69, https://doi.org/10.1016/j.compstruct.2013.07.042.
[35] M. Goodarzi, A. Amiri, M.S. Goodarzi, M.R. Safaei, A. Karimipour, E.M. Languri, M. Dahari, Investigation of heat transfer and pressure drop of a counter flow corrugated plate heat exchanger using MWCNT based nanofluids, Int. Commun. Heat. Mass Transf. 66 (2015) 172–179, https://doi.org/10.1016/j.icheatmasstransfer.2015.05.002.
[36] S. Xu, J. Liu, Q. Li, Mechanical properties and microstructure of multiwalled carbon nanotube-reinforced cement paste, Constr. Build. Mater. 76 (2015) 16–23, https://doi.org/10.1016/j.conbuildmat.2014.11.049.
[37] J. Cheon, M. Kim, Impact resistance and interlaminar shear strength enhancement of carbon fiber reinforced thermoplastic composites by introducing MWCNT-anchored carbon fiber, Compos. B Eng. 217 (2021) 108872, https://doi.org/10.1016/j.compositesb.2021.108872.
[38] D.Y. Yoo, S. Kim, G.J. Park, J.J. Park, S.W. Kim, Effects of fiber shape, aspect ratio, and volume fraction on flexural behavior of ultra-high-performance fiber-reinforced cement composites, Compos. Struct. 174 (2017) 375–388, https://doi.org/10.1016/j.compstruct.2017.04.069.
[39] S.L. Yang, S.G. Millard, M.N. Soutsos, S.J. Barnett, T.T. Le, Influence of aggregate and curing regime on the mechanical properties of ultra-high performance fibre reinforced concrete (UHPFRC), Constr. Build. Mater. 23 (6) (2009) 2291–2298, https://doi.org/10.1016/j.conbuildmat.2008.11.012.
[40] M.N. Soutsos, S.G. Millard, K. Karaiskos, Mix design, mechanical properties, and impact resistance of reactive powder concrete (RPC), Int. Workshop High. Perform. Fibre Reinf. Cem. Compos. Struct. Appl. (May 2005) 549–560. ⟨https://www.researchgate.net/publication/267794130⟩.
[41] M. Schmidt, E. Fehling, Ultra-high-performance concrete: research, development and application in Europe, Acids Spec. Publ. 228 (1) (2005) 51–78. ⟨https://www.researchgate.net/publication/264879054⟩.
[42] C. Shi, Z. Wu, J. Xiao, D. Wang, Z. Huang, Z. Fang, A review on ultra high performance concrete: part I. Raw materials and mixture design, Constr. Build. Mater. 101 (2015) 741–751, https://doi.org/10.1016/j.conbuildmat.2015.10.088.
[43] K. Pang, H. Zhou, C. Wu, H. Jiang, Z. Zhang, Y. Yu, J. Zhang, Study on behavior of waffle-type UHPC-GFRP composite slab under three-point loading, Case Stud. Constr. Mater. 19 (2023) e02457, https://doi.org/10.1016/j.cscm.2023.e0245.
[44] N.M. Azmee, N. Shafiq, Ultra-high performance concrete: from fundamental to applications, Case Stud. Constr. Mater. 9 (2018) e00197, https://doi.org/10.1016/j.cscm.2018.e00197.
[45] P. Guo, S. Mahjoubi, K. Liu, W. Meng, Y. Bao, Self-updatable AI-assisted design of low-carbon cost-effective ultra-high-performance concrete (UHPC), Case Stud. Constr. Mater. 19 (2023) e02625, https://doi.org/10.1016/j.cscm.2023.e02625.
[46] T. El-Sayed, A, Improving the performance of UHPC columns exposed to axial load and elevated temperature, Case Stud. Constr. Mater. 15 (2021) e00748, https://doi.org/10.1016/j.cscm.2021.e00748.
[47] J. Abellan-Garcia, Study of nonlinear relationships between dosage mixture design and the compressive strength of UHPC, Case Stud. Constr. Mater. 17 (2022) e01228, https://doi.org/10.1016/j.cscm.2022.e01228.
[48] Y. Bae, S. Pyo, Ultra high performance concrete (UHPC) sleeper: Structural design and performance, Eng. Struct. 210 (2020) 110374, https://doi.org/10.1016/j.engstruct.2020.110374.
[49] Y. Bae, S. Pyo, Effect of steel fiber content on structural and electrical properties of ultra high performance concrete (UHPC) sleepers, Eng. Struct. 222 (2020) 111131, https://doi.org/10.1016/j.engstruct.2020.111131.
[50] E.T. Dawood, M. Ramli, High strength characteristics of cement mortar reinforced with hybrid fibres, Constr. Build. Mater. 25 (5) (2011) 2240–2247, https://doi.org/10.1016/j.conbuildmat.2010.11.008.
[51] S.D. Salahaddin, J.H. Haido, G. Wardeh, The behavior of UHPC containing recycled glass waste in place of cementitious materials: a comprehensive review, Case Stud. Constr. Mater. 17 (2022) e01494, https://doi.org/10.1016/j.cscm.2022.e01494.
[52] S. Ahmad, I. Hakeem, A.K. Azad, Effect of curing, fibre content and exposures on compressive strength and elasticity of UHPC, Adv. Cem. Res. 27 (4) (2015) 233–239, https://doi.org/10.1680/adcr.13.00090.
[53] P. Li, L. Chen, H. Ma, G. Pan, Z. Sun, Spatial distribution characteristics and microscopic mechanisms for enhancing mechanical properties of MWCNTs in recycled coarse aggregate shotcrete, Constr. Build. Mater. 364 (2023) 129927, https://doi.org/10.1016/j.conbuildmat.2022.129927.
[54] S. Parveen, S. Rana, R. Fangueiro, et al., Microstructure and mechanical properties of carbon nanotube reinforced cementitious composites developed using a novel dispersion technique, Cem. Concr. Res. 73 (2015) 215–227, https://doi.org/10.1016/j.cemconres.2015.03.006.
[55] R.H. Baughman, A.A. Zakhidov, W.A. de Heer, Carbon nanotubes: The route towards applications, Science 297 (5582) (2002) 787–792, https://doi.org/10.1126/science.1060928.
[56] J.M. Makar, G.W. Chan, Growth of cement hydration products on single-walled carbon nanotubes, J. Am. Ceram. Soc. 92 (6) (2009) 1303–1310, https://doi.org/10.1111/j.1551-2916.2009.03055.
[57] J. Sandler, J.E. Kirk, I.A. Kinloch, M.S.P. Shaffer, A.H. Windle, Ultra-low electrical percolation threshold in carbon-nanotube-epoxy composites, Polymer 44 (19) (2003) 5893–5899, https://doi.org/10.1016/S0032-3861(03)00539-1.
[58] B. Wang, Y. Han, S. Liu, Effect of highly dispersed carbon nanotubes on the flexural toughness of cement-based composites, Constr. Build. Mater. 46 (2013) 8–12, https://doi.org/10.1016/j.conbuildmat.2013.04.014.
[59] G.M. Kim, B.J. Yang, K.J. Cho, E.M. Kim, H.K. Lee, Influences of CNT dispersion and pore characteristics on the electrical performance of cementitious composites, Compos. Struct. 164 (2017) 32–42, https://doi.org/10.1016/j.compstruct.2016.12.049.
[60] H. Lee, Y.M. Song, K.J. Loh, W. Chung, Thermal response characterization and comparison of carbon nanotube-enhanced cementitious composites, Compos. Struct. 202 (2018) 1042–1050, https://doi.org/10.1016/j.compstruct.2018.05.027.
[61] Standard Specification for Portland Cement, ASTM C 150, ASTM International, 2022.
[62] ASTM C Standard Specification for Standard Sand778, ASTM International, 2021.
[63] ASTM C 109. Standard test method for compressive strength of hydraulic cement mortars (Using 2-in, or [50-mm] cube specimens). ASTM International 2016.

[64] J. Wang, S. Dong, C. Zhou, A. Ashour, B. Han, Investigating pore structure of nano-engineered concrete with low-field nuclear magnetic resonance, J. Mater. Sci. 56 (2021) 243–259, https://doi.org/10.1007/s10853-020-05268-0.
[65] X. Wang, S. Dong, A. Ashour, W. Zhang, B. Han, Effect and mechanisms of nanomaterials on interface between aggregates and cement mortars, Constr. Build. Mater. 240 (2020) 117942, https://doi.org/10.1016/j.conbuildmat.2019.117942.
[66] B. Han, L. Zhang, S. Zeng, S. Dong, X. Yu, R. Yang, J. Ou, Nano-core effect in nano-engineered cementitious composites, Compos. Part A Appl. Sci. Manuf. 95 (2017) 100–109, https://doi.org/10.1016/j.compositesa.2017.01.008.
[67] X. Wang, S. Dong, Z. Li, B. Han, J. Ou, Nanomechanical characteristics of interfacial transition zone in nano-engineered concrete, Engineer 17 (2022) 99–109, https://doi.org/10.1016/j.eng.2020.08.025.

SK is pursuing a Doctoral degree in the Department of Civil Engineering, College of Engineering at Chosun University, Gwangju, Republic of Korea.

SP is an Associate Professor in the Department of Civil, Urban, Earth, and Environmental Engineering at Ulsan National Institute of Science and Technology (UNIST), Ulsan, Republic of Korea.

HL is an Associate Professor in the Department of Civil Engineering at Chosun University, Gwangju, Republic of Korea.